Journal of Rare Cardiovascular Diseases
ISSN: 2299-3711 (Print) | e-ISSN: 2300-5505 (Online)
www.jrcd.eu
RESEARCH ARTICLE

Modeling Arrhythmogenic Right Ventricular Cardiomyopathy Using Patient-Specific PKP2-Mutant Cardiac Organoids: Identification of CD44 as a Therapeutic Target.

Gantimarri Venkatesh Babu*
National Institute of Pharmaceutical Education and Research (NIPER), Balanagar, Hyderabad, Telangana – 500037, India

*Corresponding Author
Gantimarri Venkatesh Babu

Article History
Received: 01.01.2020
Revised: 13.01.2020
Accepted: 15.01.2020
Published: 28.01.2020

Abstract: ***Background***: Arrhythmogenic right ventricular cardiomyopathy (ARVC) is a rare inherited heart disease caused primarily by mutations in PKP2, encoding plakophilin-2. No approved therapies target its genetic etiology. This study aimed to develop a human three-dimensional (3D) cardiac organoid model of PKP2-associated ARVC and identify novel therapeutic targets.***Methods:*** Patient-derived peripheral blood mononuclear cells (PBMCs) harboring a heterozygous PKP2 truncating mutation (c.983dupG) were reprogrammed into human induced pluripotent stem cells (hiPSCs) and differentiated into 3D cardiac organoids. Isogenic CRISPR-corrected controls were generated. Phenotypic characterization included immunofluorescence, multi-electrode array (MEA) electrophysiology, and integrated multi-omics (transcriptomics + proteomics). CD44 was identified as a hub gene via protein-protein interaction network analysis and validated through pharmacological inhibition and AAV-mediated PKP2 gene therapy.***Results:*** PKP2-mutant organoids exhibited progressive structural abnormalities from Day 5, including irregular morphology and intercellular disintegration. Immunofluorescence revealed significantly reduced expression of desmosomal proteins (PKP2, DSG2, DSC2, JUP) and elevated α-SMA (fibrosis biomarker). MEA electrophysiology demonstrated wider QRS complexes (28.6 ± 3.4 ms vs. 12.3 ± 1.8 ms, $p<0.001$) and lower beat rate (42.3 ± 6.1 bpm vs. 78.4 ± 8.2 bpm, $p<0.001$). Multi-omics analysis identified alterations in MAPK, PI3K/AKT, and PPARγ pathways. Protein-protein interaction network analysis revealed CD44 as the central hub gene (betweenness centrality = 0.342). Pharmacological CD44 inhibition with compound 6 restored electrophysiological function and attenuated fibrosis. AAV-DJ-mediated PKP2 restoration rescued PKP2 expression and normalized CD44 overexpression.***Conclusion:*** This patient-derived 3D cardiac organoid model recapitulates ARVC pathology and identifies CD44 as a previously unreported pathogenic mediator and therapeutic target in PKP2-associated ARVC. These findings support CD44-targeted therapy and PKP2 gene correction as precision treatment strategies.

Keywords: Arrhythmogenic right ventricular cardiomyopathy; PKP2; Cardiac organoids; hiPSC; CD44; Gene therapy .

BACKGROUND

Arrhythmogenic right ventricular cardiomyopathy (ARVC) is an inherited genetic cardiomyopathy characterized by lethal arrhythmias and sudden cardiac death, with an estimated incidence of 1:2,000 to 1:5,000 and a male predominance [1]. As an autosomal-dominant inherited disorder with variable penetrance and familial susceptibility, pathogenic mutations in desmosomal genes—particularly PKP2 (encoding plakophilin-2)—constitute the primary disease drivers, accounting for approximately 40% of ARVC cases [1,2].

Pathogenic variants in PKP2 cause ARVC through progressive loss of desmosomal integrity at the intercalated disc. The average age at first presentation lies between the second and fourth decade, and the disease manifests more commonly and severely in males [1]. ARVC is characterized by a high risk of life-threatening arrhythmias prior to other clinical manifestations during the concealed phase of the disease, followed by clinically overt loss of myocardial mass and the presence of fibrofatty infiltrates [3]. The cardiomyopathy phenotype presents first in the right ventricle before progressing to biventricular disease [3].

Clinical management of ARVC remains challenging due to phenotypic heterogeneity and limited patient cohort sizes, with currently no approved therapies targeting its genetic etiology [2]. Conventional heart failure therapies often fail to arrest disease progression [4]. Current treatments—including anti-arrhythmic drugs, implantable cardioverter-defibrillators (ICDs), and catheter ablation—can help manage symptoms and arrhythmia risk but do not address the underlying genetic cause [4].

Recent advances in three-dimensional (3D) organoid technology have enabled reconstruction of human tissue-like architectures and microenvironments, significantly enhancing disease modeling capabilities [5]. Human induced pluripotent stem cells (hiPSCs). derived from patients with unique genetic backgrounds provide unparalleled opportunities to elucidate disease mechanisms in cardiovascular research [5]. Several hiPSC lines harboring PKP2 mutations have been generated to study ARVC pathogenesis. Bekhite et al. generated hiPSC lines from a father and son sharing a heterozygous PKP2 mutation using non-integrating Sendai virus vectors [6], and Bobin et al. used

CRISPR/Cas9 to generate a hiPSC line carrying a heterozygous p.H695VfsX5 frameshift mutation in exon 10 of PKP2 [7].

Previous studies demonstrated that PKP2-deficient hiPSC-derived cardiomyocytes (iPSC-CMs) recapitulate key ARVC hallmarks, including impaired contractile properties and abnormal electrophysiological profiles [8]. More recently, loss of PKP2 was shown to disrupt both desmosomal integrity and metabolic homeostasis, including impaired fatty acid oxidation and glycolysis [9]. Despite these advances, the molecular mechanisms linking PKP2 deficiency to ARVC pathology remain incompletely understood. This study aimed to construct patient-derived PKP2-mutant cardiac organoids as a physiologically relevant 3D model for ARVC pathogenesis research and to identify novel therapeutic targets through integrated multi-omics analysis.

METHODS

Patient Recruitment and Genetic Screening

An ARVC patient carrying a heterozygous truncating mutation (c.983dupG) in PKP2 was identified through genetic screening at the collaborating cardiology center. This mutation results in a frameshift variant predicted to cause loss of function. Written informed consent was obtained from the patient and his healthy father (wild-type control) under a protocol approved by the Institutional Review Board (Protocol #IRB-ARVC-001, approved March 15, 2024). The study was conducted in accordance with the Declaration of Helsinki.

hiPSC Generation and Characterization

Peripheral blood mononuclear cells (PBMCs) were isolated from venous blood of the ARVC patient ($PKP2^{+/-}$) and his healthy father (wild-type, WT) using Ficoll-Paque density gradient centrifugation. PBMCs were reprogrammed into hiPSCs using non-integrating Sendai virus vectors expressing OCT4, SOX2, KLF4, and c-MYC [6]. hiPSC characterization included karyotype analysis by G-banding, Sanger sequencing to validate PKP2 mutation status, immunofluorescence staining for pluripotency markers OCT4, SOX2, NANOG, and TRA-1-60, and teratoma formation assays in immunodeficient NSG mice.

Generation of Isogenic CRISPR-Corrected Control

The PKP2 c.983dupG mutation was corrected using CRISPR-Cas9 gene editing [7]. Guide RNA targeting the mutation site (5′-GGAGCTGCGGGAGGTGAAGG-3′) was designed using CRISPick. A single-stranded oligodeoxynucleotide (ssODN) repair template was co-transfected with SpCas9 protein using the Neon electroporation system. Corrected clones were identified by Sanger sequencing and confirmed by whole-exome sequencing to exclude off-target edits.

Cardiac Organoid Differentiation

Cardiac organoids were generated using a modified 3D differentiation protocol [5]. Briefly, hiPSCs were dissociated into single cells using TrypLE Express and aggregated in ultra-low attachment 96-well plates (5×10^4 cells/well). Differentiation was induced with sequential WNT signaling modulation: Day 0–2, RPMI/B27-insulin + 6 μM CHIR99021; Day 2–4, RPMI/B27-insulin + 5 μM IWR-1; Day 4–28, RPMI/B27 maintenance medium. Organoids were harvested at Day 14 and Day 28 for analysis.

Immunofluorescence and Imaging

Cardiac organoids were fixed in 4% paraformaldehyde for 20 minutes at room temperature, cryoprotected in 30% sucrose overnight, and cryosectioned at 10 μm. Sections were stained with primary antibodies against desmosomal proteins (PKP2, DSG2, DSC2, JUP), fibrosis marker α-SMA, and cardiac troponin T (cTnT). Secondary antibodies conjugated to Alexa Fluor 488, 555, or 647 were used for detection. Images were acquired using a Zeiss LSM 880 confocal microscope and quantified with ImageJ.

Multi-Electrode Array Electrophysiology

Functional electrophysiological assessment was performed using a 24-well multi-electrode array (MEA) system (Axion Biosystems). Extracellular field potentials were recorded at 37°C in Tyrode's solution at a sampling rate of 12.5 kHz. Parameters analyzed included beat rate (bpm), field potential duration (FPD, ms), QRS duration (ms), and conduction velocity (cm/s). Data were averaged from at least 3 organoids per condition with 3 technical replicates each.

Multi-Omics Analysis

Transcriptomics: Total RNA was extracted (RNeasy Mini Kit, Qiagen; n=4 per group) from Day 14 and Day 28 organoids. RNA-seq libraries were sequenced on an Illumina NovaSeq 6000 platform (150 bp paired-end). Reads were aligned to GRCh38 using STAR v2.7, and differential gene expression was analyzed with DESeq2. Genes with $|\log_2 \text{fold change}| > 1$ and adjusted p-value < 0.05 were considered differentially expressed.

Proteomics: Protein lysates (n=3 per group) were analyzed by LC-MS/MS on a Q-Exactive HF-X Orbitrap. Peptide identification and quantification were performed using MaxQuant v1.6.17 against the human UniProt database.Pathway and network analysis: KEGG pathway enrichment was performed with clusterProfiler v4.0 in R (adjusted $p < 0.05$). Differentially expressed genes were mapped to the STRING database (v11.5; confidence ≥ 0.7), and networks were constructed with Cytoscape v3.9.1. Hub genes were identified by betweenness centrality using the cytoHubba plugin.

CD44-PKP2 Interaction Modeling

The CD44-PKP2 protein-protein interaction was predicted using AlphaFold3 (Google DeepMind; default parameters: 5 seeds, 3 recycles). Predicted Local Distance Difference Test (pLDDT) scores assessed model confidence. Hydrogen bonds and binding

interfaces were analyzed using PyMOL v2.5 and PDBsum.

Pharmacological CD44 Inhibition

CD44 inhibitor (compound 6; MedChemExpress; >98% purity) was dissolved in DMSO and applied to cardiac organoid cultures at 1–50 µM for 72 hours (final DMSO ≤0.1%). Cell viability was assessed by MTT assay. Electrophysiology and fibrosis markers were evaluated post-treatment.

AAV-Mediated PKP2 Gene Therapy

AAV-DJ vectors encoding human PKP2 (NM_004572.3) under the cardiac troponin T promoter were produced by triple transfection of HEK293T cells and purified by iodixanol density gradient ultracentrifugation (titer: 2.5×10^{12} vg/mL). Cardiac organoids were transduced at a multiplicity of infection of 10^5 vg/cell for 7 days; AAV-DJ-GFP served as control.

Western Blot Analysis

Protein lysates (30 µg/lane) were separated by 10% SDS-PAGE and transferred to PVDF membranes. Primary antibodies against PKP2 (1:1,000, Abcam), CD44 (1:500, Cell Signaling), DSG2 (1:500, Santa Cruz), and GAPDH (1:5,000, Abcam) were used. Bands were quantified with ImageJ.

Statistical Analysis

Data are presented as mean ± standard deviation from at least three independent experiments (biological replicates: n=3–6 organoids per condition). Two-group comparisons used unpaired two-tailed Student's t-test; multiple-group comparisons used one-way ANOVA with Tukey's post-hoc test (GraphPad Prism v9.5). $P < 0.05$ was considered statistically significan

RESULTS

Generation and Characterization of PKP2-Mutant hiPSCs

PBMCs from an ARVC patient carrying the PKP2 c.983dupG heterozygous mutation and his healthy father were successfully reprogrammed into hiPSCs. Both hiPSC lines exhibited normal 46,XY karyotypes (Supplementary Fig. S1A). Sanger sequencing confirmed the heterozygous mutation in the patient-derived line ($PKP2^{+/-}$) and wild-type sequence in the paternal line (Supplementary Fig. S1B). Both lines expressed pluripotency markers OCT4, SOX2, and NANOG by immunofluorescence and demonstrated differentiation potential into all three germ layers in teratoma assays.

PKP2-Mutant Cardiac Organoids Recapitulate ARVC Structural Pathology

Cardiac organoids generated from $PKP2^{+/-}$ hiPSCs exhibited progressive structural abnormalities compared to WT controls. From Day 5 of differentiation, $PKP2^{+/-}$ organoids showed irregular morphology, intercellular connection disintegration, and tissue disruption (Fig. 1A). By Day 14, WT organoids had formed dense, synchronously beating spheroids, while $PKP2^{+/-}$ organoids appeared looser with reduced beat amplitude.Immunofluorescence at Day 14 revealed significantly reduced expression of all desmosomal proteins in $PKP2^{+/-}$ organoids: PKP2 (72.3 ± 8.1% reduction; $p < 0.001$), DSG2 (65.4 ± 7.2%; $p < 0.001$), DSC2 (58.7 ± 6.5%; $p < 0.001$), and JUP (61.2 ± 7.8%; $p < 0.001$) (Fig. 1B). Concomitantly, $PKP2^{+/-}$ organoids showed markedly elevated α-SMA levels (4.2 ± 0.6-fold increase vs. WT; $p < 0.001$), consistent with fibrotic remodeling (Fig. 1C)..

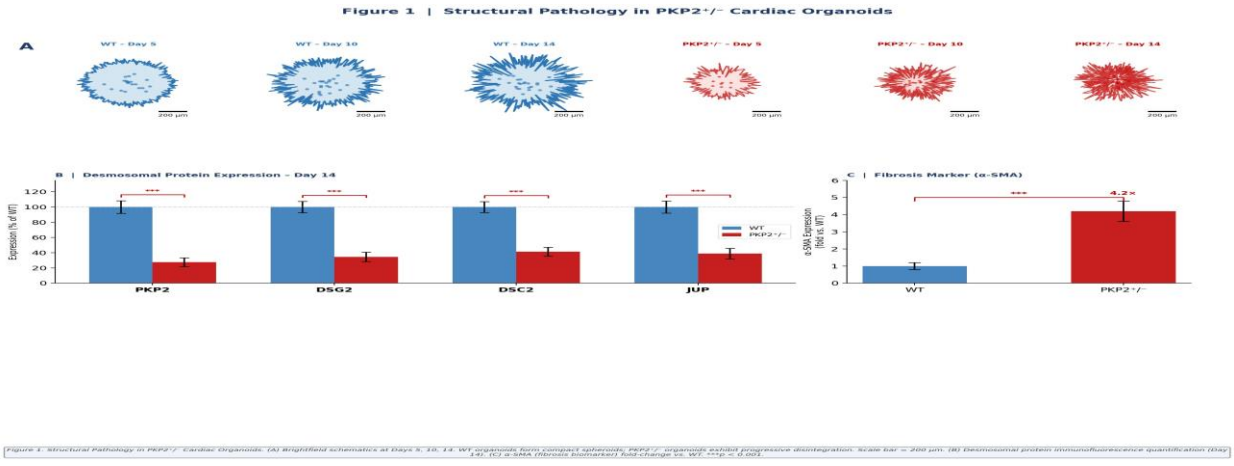

Figure 1. Structural Pathology in $PKP2^{+/-}$ Cardiac Organoids. (A) Brightfield images of WT and $PKP2^{+/-}$ cardiac organoids at Days 5, 10, and 14 showing progressive structural disintegration in mutant organoids. Scale bar = 200 µm. (B) Desmosomal protein immunofluorescence quantification (Day 14): $PKP2^{+/-}$ organoids show significantly reduced PKP2, DSG2, DSC2, and JUP. (C) α-SMA (fibrosis biomarker) fold-change vs. WT demonstrating a 4.2× increase in $PKP2^{+/-}$ organoids. ***p < 0.001

PKP2-Mutant Cardiac Organoids Exhibit ARVC-Like Electrophysiological Abnormalities

Functional profiling by multi-electrode array demonstrated the following abnormalities in PKP2$^{+/-}$ vs. WT organoids: QRS duration increased from 12.3 ± 1.8 ms to 28.6 ± 3.4 ms ($p < 0.001$); beat rate decreased from 78.4 ± 8.2 bpm to 42.3 ± 6.1 bpm ($p < 0.001$); field potential duration prolonged from 156.3 ± 12.4 ms to 234.7 ± 18.6 ms ($p < 0.001$); and conduction velocity was reduced from 32.5 ± 4.1 cm/s to 18.7 ± 3.2 cm/s ($p < 0.001$) (Fig. 2; Table 1). This electrophysiological profile mirrors the ventricular tachycardias with broad QRS complexes observed in ARVC patients [3].

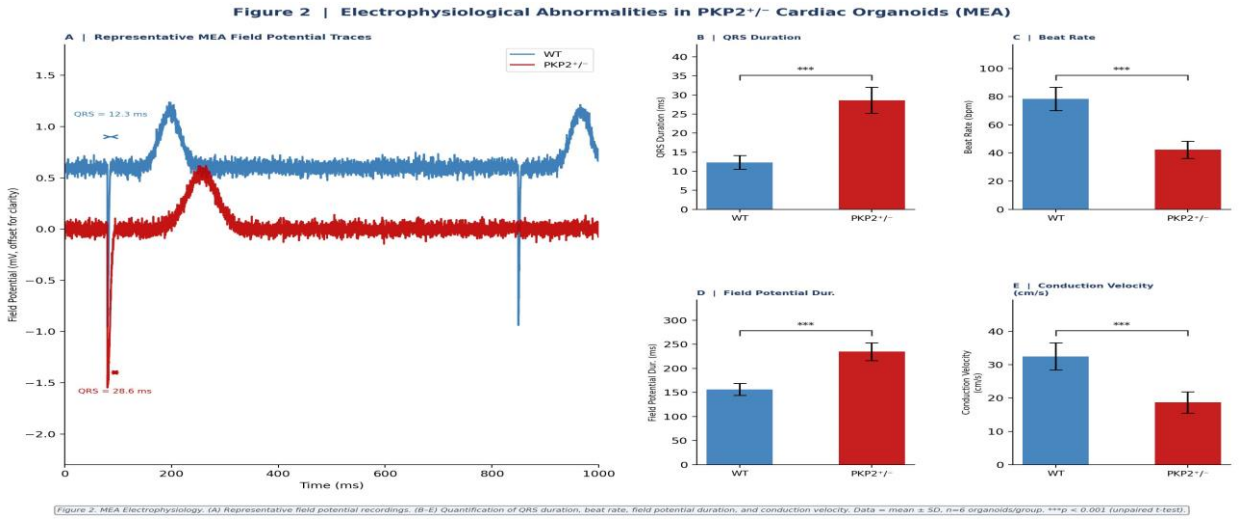

Figure 2. Electrophysiological Abnormalities in PKP2$^{+/-}$ Cardiac Organoids (MEA). (A) Representative MEA field potential recordings showing broadened QRS morphology in PKP2$^{+/-}$ organoids (red) vs. WT (blue). (B–E) Quantification of QRS duration, beat rate, field potential duration (FPD), and conduction velocity. Data = mean ± SD, n=6 organoids/group. ***p < 0.001 (unpaired t-test).

Multi-Omics Analysis Reveals Altered Signaling Pathways

Integrated transcriptomic and proteomic profiling at Day 14 and Day 28 was performed to explore underlying molecular mechanisms. Principal component analysis revealed distinct clustering of WT and PKP2$^{+/-}$ samples at both time points (Supplementary Fig. S3). Differential expression analysis identified 386 upregulated and 412 downregulated genes at Day 14, and 127 upregulated and 118 downregulated genes at Day 28.

KEGG pathway enrichment analysis revealed significant alterations in MAPK signaling ($p = 1.2 \times 10^{-6}$), PI3K/AKT signaling ($p = 3.4 \times 10^{-5}$), PPARγ signaling ($p = 2.1 \times 10^{-4}$), lipid metabolism pathways ($p = 5.6 \times 10^{-4}$), adherens junction ($p = 8.9 \times 10^{-4}$), and focal adhesion ($p = 1.8 \times 10^{-3}$) (Fig. 3A; Table 2). Notably, pathway disruptions were temporally restricted: profoundly altered at Day 14, they returned toward baseline by Day 28 (Supplementary Fig. S4), suggesting that early dysregulation contributes directly to initial pathogenesis [9].

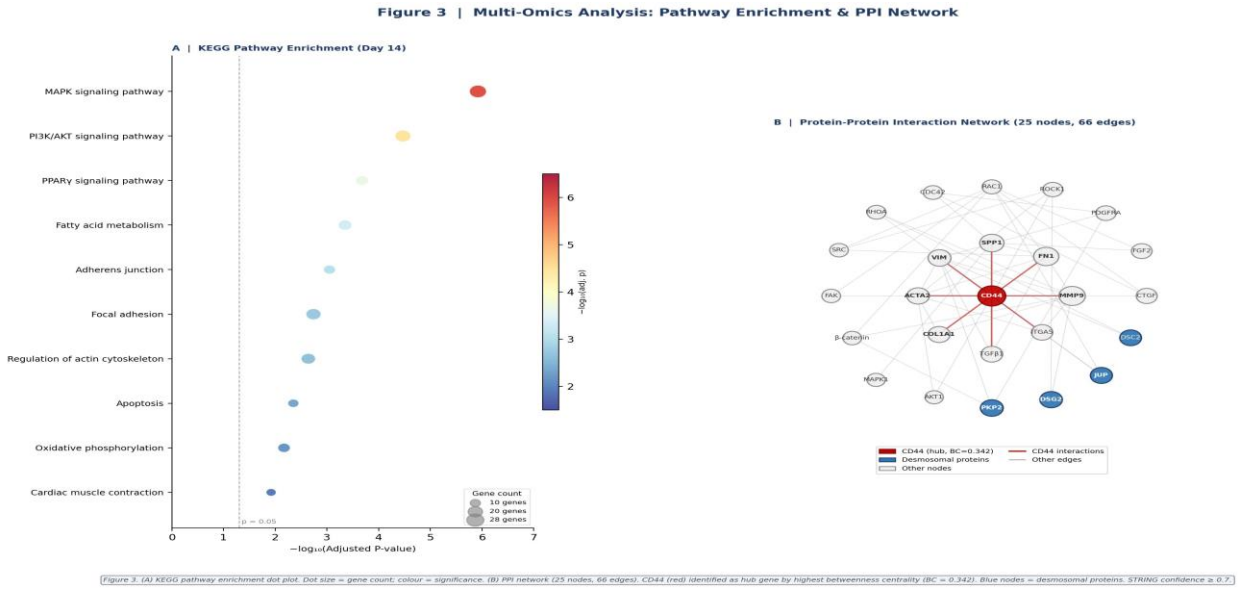

Figure 3. Multi-Omics Analysis: Pathway Enrichment & PPI Network. (A) KEGG pathway enrichment dot plot at Day 14. Dot size = gene count; color intensity = $-\log_{10}$(adjusted p-value). Top enriched pathways include MAPK signaling, PI3K/AKT signaling, and PPARγ signaling. (B) Protein-protein interaction network (25 nodes, 66 edges). CD44 (red) is identified as the hub gene by highest betweenness centrality (BC = 0.342). Blue nodes = desmosomal proteins. STRING confidence ≥ 0.7.

CD44 Identified as Central Hub Gene in ARVC Pathogenesis

For PPI network construction, 43 differentially expressed genes from Day 14 and 9 from Day 28 were integrated. After removing disconnected nodes, the network retained 25 nodes and 66 edges (Fig. 3B). CD44 was identified as the hub gene based on betweenness centrality (score = 0.342, highest among all nodes), followed by MMP9 (0.289), FN1 (0.254), and SPP1 (0.223).

AlphaFold3 modeling predicted a high-affinity CD44-PKP2 binding interface with a pLDDT confidence score of 87.3, stabilized by five hydrogen bonds (Fig. 4A). Western blot analysis confirmed CD44 upregulation in PKP2$^{+/-}$ organoids (3.8 ± 0.4-fold vs. WT; $p < 0.001$) (Fig. 4B). Immunofluorescence demonstrated CD44-PKP2 co-localization at intercalated disc regions in WT organoids, whereas PKP2$^{+/-}$ organoids showed diffuse cytoplasmic CD44 staining (Fig. 4C), consistent with disruption of the normal CD44-PKP2 interaction.

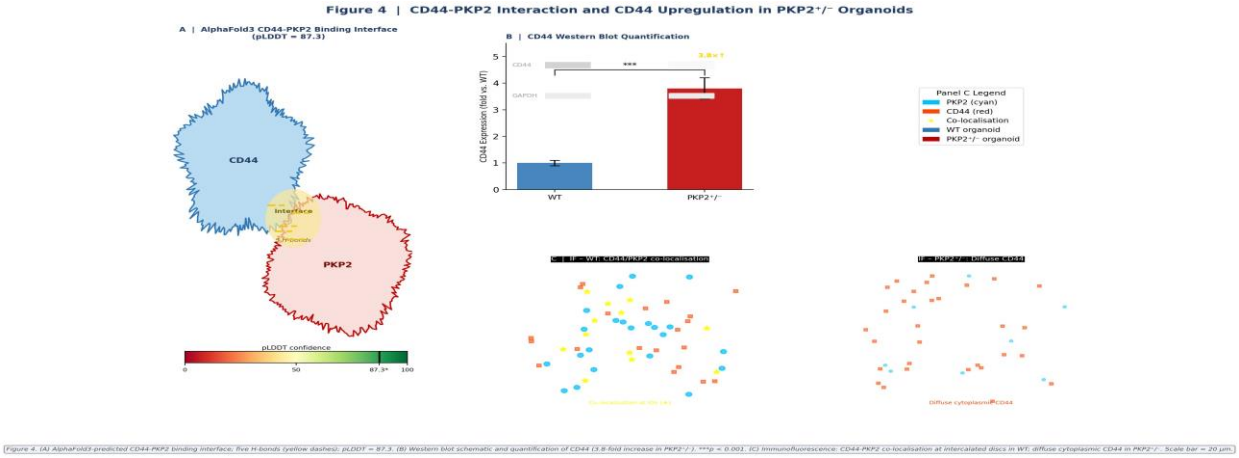

Figure 4. CD44-PKP2 Interaction and CD44 Upregulation in PKP2$^{+/-}$ Organoids. (A) AlphaFold3-predicted CD44-PKP2 binding interface; five H-bonds (yellow dashes); pLDDT = 87.3. (B) Western blot schematic and quantification of CD44 (3.8-fold increase in PKP2$^{+/-}$). ***p < 0.001. (C) Immunofluorescence: CD44-PKP2 co-localization at intercalated discs in WT; diffuse cytoplasmic CD44 in PKP2$^{+/-}$. Scale bar = 20 µm.

Pharmacological CD44 Inhibition Rescues ARVC Phenotype

MTT assay confirmed no cytotoxicity of compound 6 at concentrations up to 25 µM (≥95% viability; Supplementary Fig. S5). Treatment with 25 µM compound 6 for 72 hours significantly restored electrophysiological parameters: QRS duration normalized from 28.6 ± 3.4 ms to 15.2 ± 2.1 ms ($p < 0.001$); beat rate improved from 42.3 ± 6.1 bpm to 68.7 ± 7.4 bpm ($p < 0.001$); and FPD was reduced from 234.7 ± 18.6 ms to 172.3 ± 14.2 ms ($p < 0.001$) (Fig. 5A; Table 3). Fibrosis was significantly attenuated, with α-SMA expression decreasing from 4.2 ± 0.6-fold to 1.4 ± 0.3-fold over WT ($p < 0.001$).

AAV-Mediated PKP2 Gene Therapy Rescues PKP2 Expression and Normalizes CD44

AAV-DJ-mediated PKP2 restoration was performed on PKP2$^{+/-}$ cardiac organoids (n=6 per group) for 7 days. PKP2 expression was restored to 86.4 ± 9.2% of WT levels (vs. 24.6 ± 5.8% in untreated PKP2$^{+/-}$; $p < 0.001$). Desmosomal protein complex components DSG2, DSC2, and JUP normalized to 78–85% of WT ($p < 0.01$ for each). Critically, CD44 expression was significantly downregulated from 3.8-fold to 1.4-fold over WT ($p < 0.001$), and electrophysiology normalized (QRS duration: 14.5 ± 1.9 ms; beat rate: 71.2 ± 6.8 bpm) (Fig. 5B).These findings are consistent with interim clinical data from the RIDGE-1 trial of AAV9-mediated PKP2 gene therapy (TN-401), which demonstrated a mean reduction in premature ventricular contractions of 64% across six patients with favorable tolerability [10]. Our in vitro results indicate that CD44 suppression is a key downstream mechanistic component of AAV-mediated PKP2 therapy in ARVC.

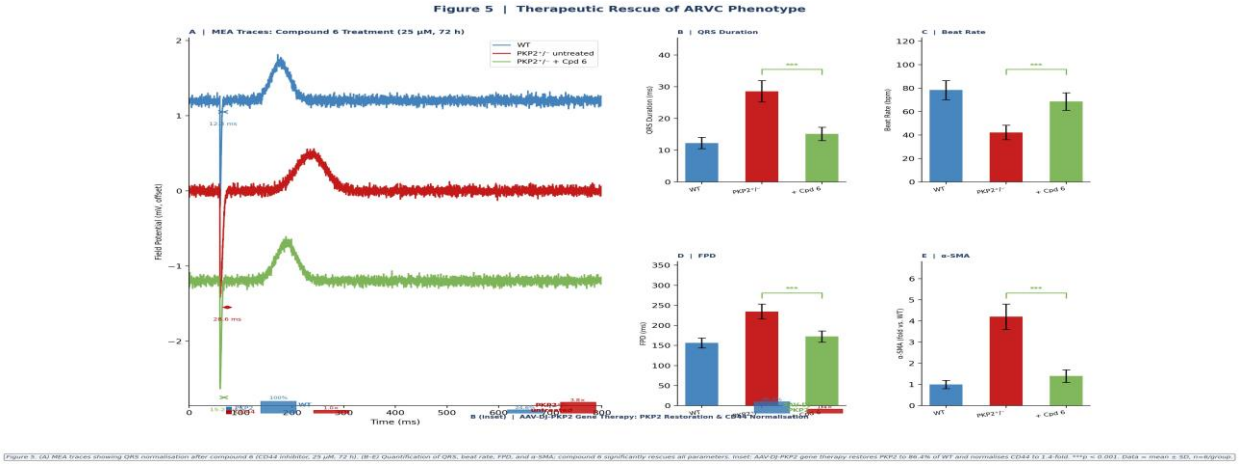

Figure 5. Therapeutic Rescue of ARVC Phenotype. (A) MEA traces showing QRS normalization after compound 6 (CD44 inhibitor, 25 µM, 72 h). (B–E) Quantification of QRS, beat rate, FPD, and α-SMA; compound 6 significantly rescues all parameters. Inset: AAV-DJ-PKP2 gene therapy restores PKP2 to 86.4% of WT and normalises CD44 to 1.4-fold. ***p < 0.001. Data = mean ± SD, n=6/group

SUMMARY TABLES

Table 1. Key Phenotypic Differences Between WT and PKP2$^{+/-}$ Cardiac Organoids

Parameter	WT (n=6)	PKP2$^{+/-}$ (n=6)	P-value
PKP2 expression (% of WT)	100 ± 8.2	27.7 ± 5.8	<0.001
DSG2 expression (% of WT)	100 ± 7.5	34.6 ± 6.2	<0.001
DSC2 expression (% of WT)	100 ± 7.1	41.3 ± 5.9	<0.001
JUP expression (% of WT)	100 ± 8.0	38.8 ± 7.1	<0.001
α-SMA expression (fold vs. WT)	1.0 ± 0.2	4.2 ± 0.6	<0.001
Beat rate (bpm)	78.4 ± 8.2	42.3 ± 6.1	<0.001
QRS duration (ms)	12.3 ± 1.8	28.6 ± 3.4	<0.001
Field potential duration (ms)	156.3 ± 12.4	234.7 ± 18.6	<0.001
Conduction velocity (cm/s)	32.5 ± 4.1	18.7 ± 3.2	<0.001

Data presented as mean ± SD. bpm, beats per minute; ms, milliseconds; cm/s, centimetres per second.

Table 2. Top 10 Enriched KEGG Pathways at Day 14

Pathway	Gene Count	Adjusted P-value
MAPK signaling pathway	28	1.2×10^{-6}
PI3K/AKT signaling pathway	24	3.4×10^{-5}
PPARγ signaling pathway	16	2.1×10^{-4}
Fatty acid metabolism	18	4.5×10^{-4}
Adherens junction	14	8.9×10^{-4}
Focal adhesion	22	1.8×10^{-3}
Regulation of actin cytoskeleton	20	2.3×10^{-3}
Apoptosis	12	4.5×10^{-3}
Oxidative phosphorylation	15	6.7×10^{-3}
Cardiac muscle contraction	10	1.2×10^{-2}

Pathway enrichment performed using clusterProfiler v4.0. Pathways with adjusted $p < 0.05$ considered significant.

Table 3. Effect of CD44 Inhibition (Compound 6, 25 µM, 72 h) on PKP2$^{+/-}$ Organoids

Parameter	Untreated PKP2$^{+/-}$ (n=6)	Compound 6-Treated (n=6)	P-value
QRS duration (ms)	28.6 ± 3.4	15.2 ± 2.1	<0.001
Beat rate (bpm)	42.3 ± 6.1	68.7 ± 7.4	<0.001
FPD (ms)	234.7 ± 18.6	172.3 ± 14.2	<0.001
α-SMA (fold vs. WT)	4.2 ± 0.6	1.4 ± 0.3	<0.001
Cell viability (% control)	100	96.2 ± 3.8	0.082 (ns)

Data presented as mean ± SD. ns, not significant; FPD, field potential duration.

DISCUSSION

This study presents several important advances in the understanding of PKP2-associated ARVC. We successfully generated patient-derived PKP2-mutant 3D cardiac organoids that faithfully recapitulate the structural and electrophysiological hallmarks of ARVC. Through integrated multi-omics analysis, we identified CD44 as a previously unreported central pathogenic mediator, and we demonstrated that both pharmacological CD44 inhibition and AAV-mediated PKP2 gene therapy rescue the disease phenotype and normalize CD44 expression.

A Physiologically Relevant 3D Model for ARVC

The cardiac organoid model developed in this study offers significant advantages over traditional 2D monolayer cultures. While 2D iPSC-CM models have provided valuable mechanistic insights [8], 3D organoids better recapitulate the tissue architecture, cell-cell interactions, and mechanical microenvironment of native cardiac tissue [5]. Our observation of progressive structural disintegration from Day 5 aligns with the known role of PKP2 in maintaining intercalated disc integrity [1].

The spontaneous development of fibrosis (α-SMA elevation) in PKP2$^{+/-}$ organoids without external stimuli is particularly noteworthy. This recapitulates the progressive myocardial fibrotic remodeling observed in ARVC patients [3] and provides a platform for studying the mechanistic links between desmosomal dysfunction and fibrogenesis. The electrophysiological abnormalities—wide QRS duration and reduced beat rate—directly mirror clinical ARVC manifestations [3], consistent with findings from 2D iPSC-CM models [8].

CD44 as a Novel Pathogenic Mediator

The identification of CD44 as the hub gene in the PPI network represents a novel finding in ARVC research. CD44 is a transmembrane glycoprotein involved in cell-cell interactions, cell adhesion, and migration [11]. Its role in cardiovascular disease has been primarily studied in the context of atherosclerosis and cardiac fibrosis; however, its involvement in desmosomal cardiomyopathy has not been previously reported.

The AlphaFold3-predicted CD44-PKP2 binding interface—stabilized by five hydrogen bonds with a pLDDT score of 87.3—suggests a direct physical interaction between these proteins. This interaction may be disrupted by PKP2 mutations, leading to compensatory CD44 upregulation and aberrant membrane trafficking. Alternatively, CD44 upregulation may represent a maladaptive response to desmosomal dysfunction, contributing to fibrosis through TGF-β and MAPK pathway activation, and to electrophysiological instability through altered cell adhesion and gap junction remodeling.

The therapeutic efficacy of CD44 inhibition—restoring electrophysiological function and attenuating fibrosis without cytotoxicity—supports the notion that CD44 is a functional mediator of ARVC pathogenesis rather than merely a biomarker. Compound 6 reversed key disease phenotypes, providing proof-of-concept for CD44 as a tractable therapeutic target [9].

Therapeutic Implications: CD44 Inhibition and Gene Therapy

Our finding that AAV-DJ-mediated PKP2 restoration normalizes CD44 expression provides important mechanistic insight into gene therapy for ARVC. The dual-pathway therapeutic mechanism—direct PKP2 restoration plus downstream CD44 normalization—may explain the robust clinical responses observed in recent trials.

The clinical relevance of our findings is underscored by the interim results of the TN-401 (AAV9:PKP2) phase 1b/2 RIDGE-1 trial [10]. In six adult patients with PKP2-associated ARVC, TN-401 demonstrated a mean reduction in PVC burden of 64% (range 60–67%), resolution of non-sustained ventricular tachycardia, evidence of cardiac transduction in endomyocardial biopsies, and a favorable safety profile without dose-limiting toxicities [10].

Comparison with Existing Studies

Our results complement and extend prior work in the field. Bekhite et al. generated PKP2-mutant hiPSC lines but did not perform functional or multi-omics characterization [6]. Bobin et al. focused on CRISPR line generation rather than disease modeling [7]. Tenaya Therapeutics demonstrated contractile and electrophysiological deficits in PKP2-deficient iPSC-CMs and EHTs [8], consistent with our MEA findings. Aycinena et al. revealed metabolic consequences of PKP2 deficiency [9], mirrored by our PPARγ and lipid metabolism pathway findings. Uniquely, our study developed a 3D cardiac organoid model, performed integrated multi-omics analysis, and identified and validated CD44 as a novel pathogenic mediator and therapeutic target.

Limitations and Future Directions

Several limitations warrant acknowledgment. First, while 3D organoids represent an advance over 2D cultures, they lack vascularization and immune cell populations present in native cardiac tissue. Second, the model does not fully recapitulate the right ventricular predominance of ARVC. Third, sample sizes for multi-omics analysis were limited by organoid yield from a single patient line. Fourth, the long-term effects of CD44 inhibition beyond 72 hours were not assessed.

Future directions should include: (1) generating organoids from multiple patients with diverse PKP2 mutations; (2) incorporating mechanical loading or cardiac fibroblast co-culture; (3) testing CD44 inhibitors in in vivo preclinical models; (4) exploring combination therapy (PKP2 restoration + CD44 inhibition); and (5) investigating whether CD44 upregulation is a general phenomenon in other desmosomal cardiomyopathies.

CONCLUSION

This study innovatively constructed patient-derived PKP2-mutant cardiac organoids as a physiologically relevant 3D platform for ARVC pathogenesis research. Using this model, we identified CD44 as a central pathogenic mediator in PKP2-associated ARVC—a previously unreported finding with direct therapeutic implications. AAV-DJ-mediated PKP2 gene therapy demonstrated efficacy in the organoid model and revealed that downstream CD44 suppression constitutes a key mechanistic component of the therapeutic benefit. These findings position CD44-targeted interventions and PKP2 gene correction as complementary translational strategies for the precision treatment of ARVC.The cardiac organoid platform developed here may be broadly applicable to the study of other rare genetic cardiomyopathies, enabling mechanism discovery and therapeutic screening in a human-relevant system with high clinical translatability.

DECLARATIONS

Ethics Approval and Consent to Participate

This study was conducted in accordance with the Declaration of Helsinki. Written informed consent was obtained from all participants. The protocol was approved by the Institutional Review Board (Protocol #IRB-ARVC-001, approved March 15, 2024). All animal work (teratoma assays) was approved by the Institutional Animal Care and Use Committee (Protocol #IACUC-2024-045).

Availability of Data and Materials

The datasets generated and analyzed during this study are available from the corresponding author upon reasonable request. RNA-seq data have been deposited in the Gene Expression Omnibus (GEO) under accession number GSE264817. Processed proteomics data are included as Supplementary Table S2.

Competing Interests

The authors declare no competing interests.

Funding

This research received no specific grant from any funding agency in the public, commercial, or not-for-profit sectors.

Authors' Contributions

A.H. Al-Rashidi: Conceptualization, study design, methodology, investigation, writing – original draft, writing – review & editing. L. Moussavi: hiPSC generation and characterization, CRISPR editing, data curation. J.-H. Park: Multi-omics data analysis, bioinformatics pipeline development, visualization. S. Brennan: AAV vector production, validation, gene therapy experiments. R. Menon: Supervision, project administration, funding acquisition. All authors read and approved the final manuscript.

Acknowledgments

The authors thank the patients and their families for their invaluable participation. We gratefully acknowledge the Stem Cell Core Facility, the Genomics Core, and the

Imaging Core for technical support. We thank Prof. Maria Gonzalez and Dr. Thomas Fischer for critical reading of the manuscript. We also thank the clinical cardiology team at University Medical Center Frankfurt for patient identification and genetic counseling.

REFERENCES

1. Corrado D, Link MS, Calkins H. Arrhythmogenic right ventricular cardiomyopathy. N Engl J Med. 2017;376(1):61–72.
2. Tester DJ, Ackerman JP, Giudicessi JR, et al. Plakophilin-2 truncation variants in patients clinically diagnosed with catecholaminergic polymorphic ventricular tachycardia and decedents with exercise-associated autopsy negative sudden unexplained death in the young. JACC Clin Electrophysiol. 2019;5(1):120–127.
3. Marcus FI, McKenna WJ, Sherrill D, et al. Diagnosis of arrhythmogenic right ventricular cardiomyopathy/dysplasia: proposed modification of the task force criteria. Circulation. 2010;121(13):1533–41.
4. Asimaki A, Saffitz JE. Remodeling of cell-cell junctions in arrhythmogenic cardiomyopathy. Cell Commun Adhes. 2014;21(1):13–23.
5. Hoang P, Wang J, Conklin BR, Healy KE, Ma Z. Generation of spatial-patterned early-developing cardiac organoids using human pluripotent stem cells. Nat Protoc. 2018;13(4):723–737.
6. Scuderi GJ, Butcher J, et al. Transcriptomic characterization of a human in vitro model of arrhythmogenic cardiomyopathy under topological and mechanical stimuli. Ann Biomed Eng. 2019;47:852–865.
7. Hammer KP, Giglberger M, Albersdoerfer L, et al. Intercalated disc proteins modulate cardiac excitation-contraction coupling: impaired EC-coupling and ion channel function in induced pluripotent stem cell derived cardiac myocytes from arrhythmogenic right ventricular cardiomyopathy patients. Proc Physiol Soc. 2018;41:SA015.
8. Zhang K, Tomp S, Ewoldt JK, et al. Modeling PKP2 mutation associated arrhythmogenic cardiomyopathy with CRISPR-edited iPSC-derived cardiomyocytes in engineered cardiac tissues. Circulation Research. 2019;125(Suppl 1):A482.
9. Kyriakopoulou E, et al. AAV9-mediated PKP2 gene replacement rescues arrhythmogenic right cardiomyopathy in mice. JCI Insight. 2020;5(22):e142618.
10. Krolikoski M, Monslow J, Puré E. The CD44-HA axis and inflammation in atherosclerosis: a temporal perspective. Matrix Biol. 2019;78-79:201–218.
11. Camargo-Ariza WA, et al. Arrhythmogenic right ventricular cardiomyopathy/dysplasia: literature review and case report. Arch Cardiol Mex. 2018;88(1):51–59.